

MILLING FORCE PREDICTION CASE STUDY FOR NON-STANDARD GEOMETRY ENDMILL USING STRUCTURED LIGHT SCANNING

Timothy No¹, Michael Gomez², and Tony Schmitz^{1,2}

¹Department of Mechanical, Aerospace, and Biomedical Engineering
University of Tennessee, Knoxville
Knoxville, TN, 37996, USA

²Manufacturing Science Division
Oak Ridge National Laboratory
Oak Ridge, TN, 37830, USA

INTRODUCTION

The ability to model and predict milling forces enables the selection of optimal machining parameters. While feasible for endmills with standard cutting edge geometries, non-standard geometry endmills prove more difficult to accurately model. The main limitation is not knowing the location and radii of the cutting edges along the cutting edge length. This issue has been addressed using a structured light scanner to generate a 3D model of the endmill. From the model, the tool-specific cutting edge geometry is identified and used to predict milling behavior by time domain simulation.

Examples of non-standard geometries include serrated cutting edges, variable pitch, variable helix, and inserted/indexable endmills. The tool selected for this case study was a 12.7 mm diameter, four flute, solid carbide, square endmill, with two smooth and two serrated helical cutting edges arranged in an alternating pattern (Iscar FINISHRED™, part number 5622230). The tool design specifications were determined from the reverse engineering capabilities of the structured light scanner.

Two methods were applied to determine the force model. First, experimental cutting forces were measured with a cutting force dynamometer at prescribed machining parameters and the force model coefficients were extracted by performing a linear regression of the mean cutting forces. Second, finite element cutting simulations were performed, which incorporated the rake and relief

profile of the cutting edge, to predict the orthogonal cutting force components and determine the force model coefficients. The cross-sectional profile was obtained from the tool scan.

The time domain simulation incorporates the cutting edge measurements from the scan, the force model coefficients derived from experimental cutting tests and finite element cutting simulations, and the tool point structural dynamics in order to predict the cutting forces. The milling force predictions were validated with measured cutting forces.

This paper builds on prior efforts utilizing structured light scanning to determine tool specific geometries in a digital modeling approach to predict milling forces [1-9].

SCANNING METROLOGY

A structured light scanner was used to generate a 3D model of the endmill. The scanning proceeded by first preparing the solid carbide endmill surface using a removable anti-glare coating. Reference targets were placed onto the surface of the rotary table to enable multiple scans to be stitched together and to generate the solid 3D model. The endmill and 3D model are displayed in Fig. 1. The coordinate system was established by fitting a cylinder to the tool shank and defining a plane at the fluted end's extreme point. The intersection of the cylinder's axis and the plane was set as the origin of the coordinate system. The edge coordinates and scale of the

² Notice: This manuscript has been authored by UT-Battelle, LLC, under contract DE-AC05-00OR22725 with the US Department of Energy (DOE). The US government retains and the publisher, by accepting the article for publication, acknowledges that the US government retains a nonexclusive, paid-up, irrevocable, worldwide license to publish or reproduce the published form of this manuscript, or allow others to do so, for US government purposes. DOE will provide public access to these results of federally sponsored research in accordance with the DOE Public Access Plan (<http://energy.gov/downloads/doe-public-access-plan>).

tool scan are shown in Fig. 2. The GOM ATOS Q system was used for this research.

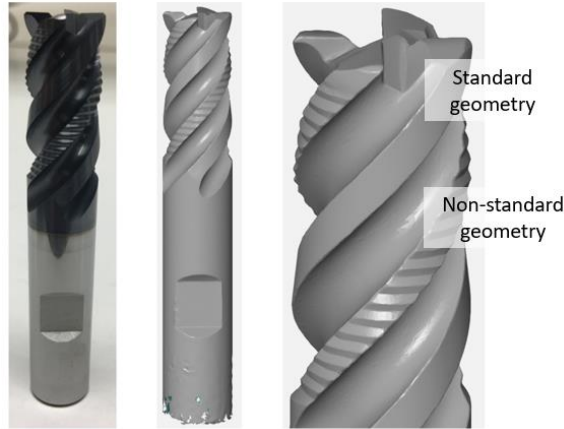


FIGURE 1. Iscar endmill and 3D model.

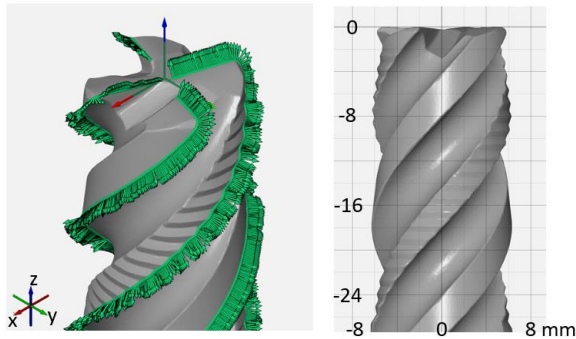


FIGURE 2. (Left) Edge coordinates and (Right) scale of scanned tool.

The edge radius values as a function of the z (axial) location are displayed in Fig. 3. The different radial profiles for the two different teeth geometries are observed (standard and serrated cutting edges). It can be seen that the serration profile of tooth 2 and tooth 4 are offset by 180 degrees. The angle values are shown in Fig. 4. The tooth spacing is 90 deg.

Planar cross-sections were created along the tool's axis (z direction). Each cross-section contained the rake and relief profiles of each tooth at the corresponding axial location; an example cross-section is displayed in Fig. 5.

TIME DOMAIN SIMULATION DESCRIPTION

Time domain simulation enables numerical solution of the coupled, second-order, time-delay differential equations of motion for milling in small time steps [10]. It is well suited to incorporating the inherent complexities of milling dynamics,

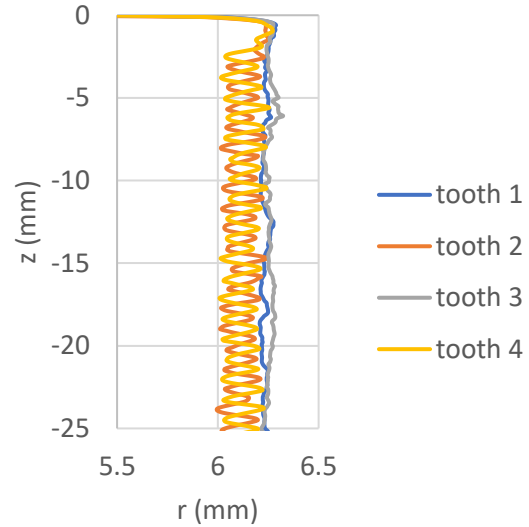


FIGURE 3. Iscar endmill radius values for the four teeth as a function of the z location along the tool axis.

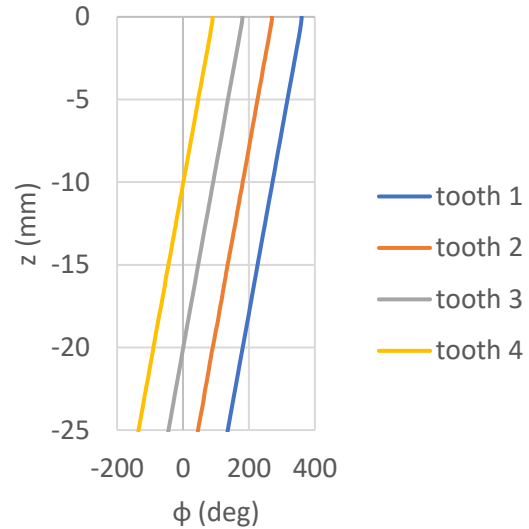


FIGURE 4. Iscar endmill angle values for the four teeth as a function of the z location along the tool axis.

including complicated tool geometries (runout of the cutter teeth, non-uniform teeth spacing, variable helix, and indexable geometries) and the nonlinearity that occurs if the tooth leaves the cut due to large magnitude vibrations. As opposed to analytical or semi-analytical stability maps that provide a global picture of the stability behavior, time domain simulation provides information regarding the local cutting force and vibration behavior for the selected cutting conditions.

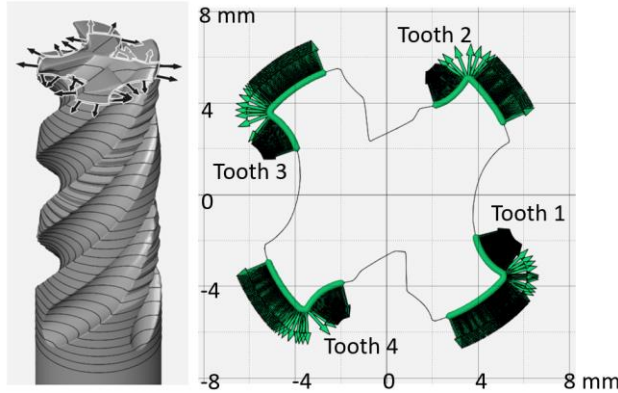


FIGURE 5. (Left) Planar cross-section for 3D model. (Right) Cross-section showing rake and relief faces for all four teeth.

The time domain simulation directly incorporates the measured tooth angles and radius variation from the tool scan. The radius variation for each tooth is included as runout, RO. Given this information, the simulation proceeds as follows:

1. The instantaneous chip thickness, $h(t)$, is determined using the commanded chip thickness, runout, and vibration of the current and previous teeth at the selected tooth angle for the current axial slice.
2. The cutting force components in the tangential, t , and normal, n , directions are calculated at each axial slice using the cutting force coefficients obtained from finite element analysis:

$$F_t(t) = k_{tc}bh(t) + k_{te}b \quad (1)$$

$$F_n(t) = k_{nc}bh(t) + k_{ne}b \quad (2)$$

where b is the axial slice width and the cutting force coefficients are identified by the subscripts t or n for direction and c or e for cutting or edge. These forces are then summed over all axial slices engaged in the cut.

3. The summed force components are used to find the new displacements by numerical integration of the second-order differential equations of motion in the x (feed) and y directions:

$$m_x\ddot{x} + c_x\dot{x} + k_x x = F_t(t)\cos\phi + F_n(t)\sin\phi \quad (3)$$

$$m_y\ddot{y} + c_y\dot{y} + k_y y = F_t(t)\sin\phi - F_n(t)\cos\phi \quad (4)$$

where m is the modal mass, c is the modal viscous damping coefficient, and k is the modal stiffness. The subscripts (x or y) identify the direction. While these equations

include only a single degree of freedom in each direction, multiple degrees-of-freedom in each direction can be accommodated by summing the modal contributions.

4. The tool rotation angle is incremented, and the process is repeated.

FORCE MODELING

For this case study, the four cutting force coefficients from Eqs. 1 and 2 were identified using two methods: 1) experimentally using the average force, linear regression approach [10]; and 2) using AdvantEdge™ finite element software and the proprietary 6061-T6 aluminum flow stress model.

For the first method, down milling tests were completed for: 3.18 mm radial depth, 5 mm axial depth, 5000 rpm spindle speed, and six feed per tooth values with the 6061-T6 workpiece mounted on a cutting force dynamometer. The mean force in the x (feed) and y directions was plotted against the commanded feed per tooth and linear regressions were completed. The slope and intercept values were then used to determine the cutting force coefficients. Three trials of these variable feed cutting tests were completed.

For the second method, the following procedure was followed to calculate the cutting force coefficients:

1. The proprietary 6061-T6 material model was selected. The tool material was set as carbide.
2. The cutting edge cross-sectional geometry was imported as a series of points that defined the rake and relief profiles.
3. The orthogonal cutting parameters were specified including the cutting speed, chip width, and chip thickness.
4. The simulation was completed and the mean feed direction, F_t , and surface normal direction, F_n , force values were recorded (initial transients at cut entry and final transients at cut exit were excluded).
5. The force coefficients were calculated by dividing the mean force components by the uncut chip area (i.e., the product of the chip width and chip thickness).
6. The chip thickness was modified and steps 4 and 5 were repeated.

A comparison between the experimental (average force, linear regression, AFLR) and AdvantEdge™ (finite element, FE) coefficients is

provided in Figs. 6 and 7. The error bars on the AFLR values represent \pm three standard deviations obtained from three repeated trials where all six cutting tests were completed (at each feed per tooth value). There are no uncertainty intervals for the FE values because the proprietary flow stress model was applied in the finite element calculations and the model type and coefficients were unknown.

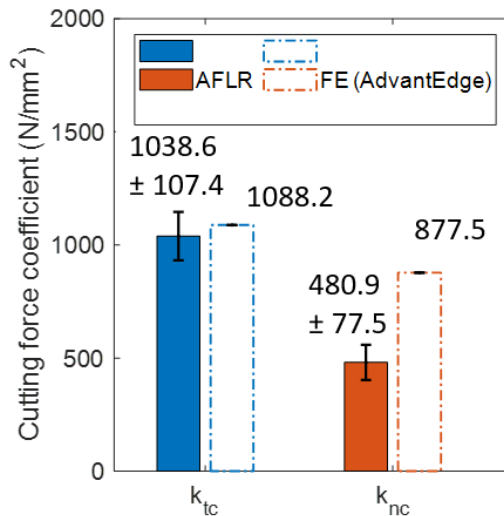


FIGURE 6. Cutting coefficients from Eqs. 1 and 2 obtained by average force linear regressions (AFLR) and finite element (FE) analysis.

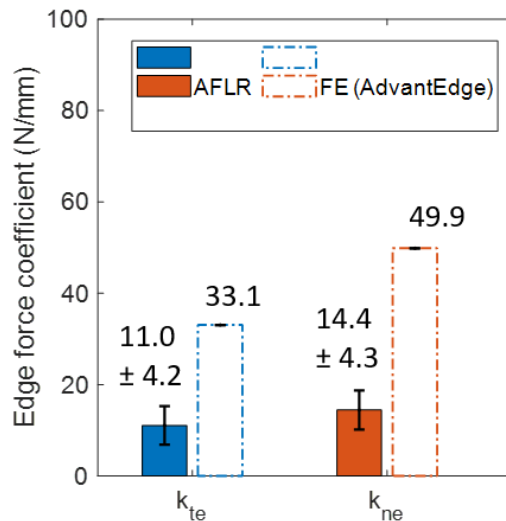


FIGURE 7. Edge coefficients from Eqs. 1 and 2 obtained by average force linear regressions (AFLR) and finite element (FE) analysis.

CUTTING FORCE COMPARISON

Cutting tests were completed on the Haas VF-4 CNC milling machine. The 6061-T6 aluminum workpiece was mounted on a Kistler 9257B

cutting force dynamometer; the endmill was clamped in the collet holder and inserted in the CAT-40 spindle interface; see Fig. 8.

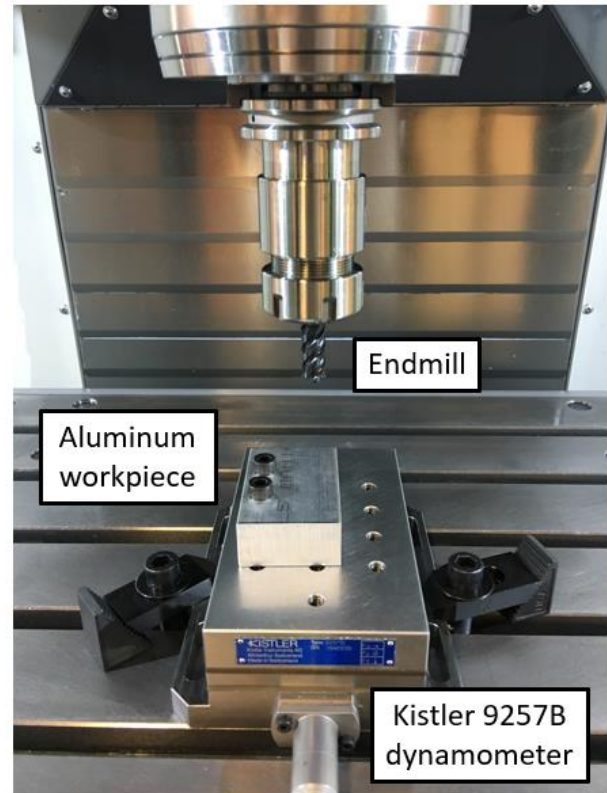


Figure 8. Experimental setup for Iscar endmill cutting force measurement.

The tool tip and workpiece FRFs were measured by impact testing. The FRFs are displayed in Fig. 9. No significant vibration modes were identified for the workpiece. The tool tip FRFs were fit and the modal parameters were used in the time domain simulation.

Down milling tests were performed at a radial depth of 6.35 mm (50% radial immersion), feed per tooth value of 0.075 mm/tooth, 5000 rpm spindle speed, and the axial depth was varied from 2 mm to 8 mm in steps of 2 mm. The predicted and measured x and y direction forces are displayed in Fig. 10 through 13. Results for both force models are included: 1) the average force, linear regression results are represented by \pm three standard deviation error bounds (green filled range); and 2) the finite element-based force model predictions are represented by the dotted blue line. The experimental results are identified by the red dash-dot line.

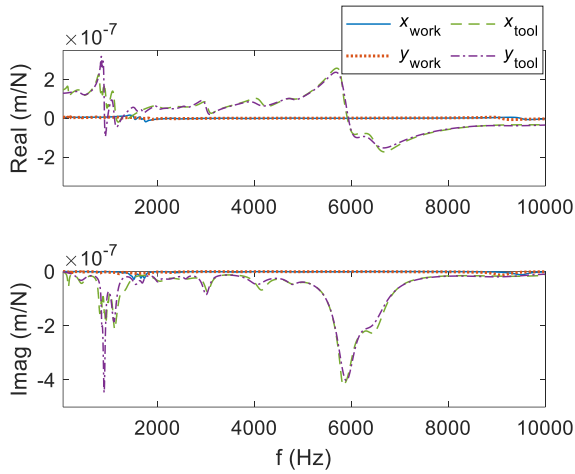


FIGURE 9. Tool tip and workpiece FRFs for the x and y directions. The (top) real and (bottom) imaginary parts of the complex-valued FRFs are presented.

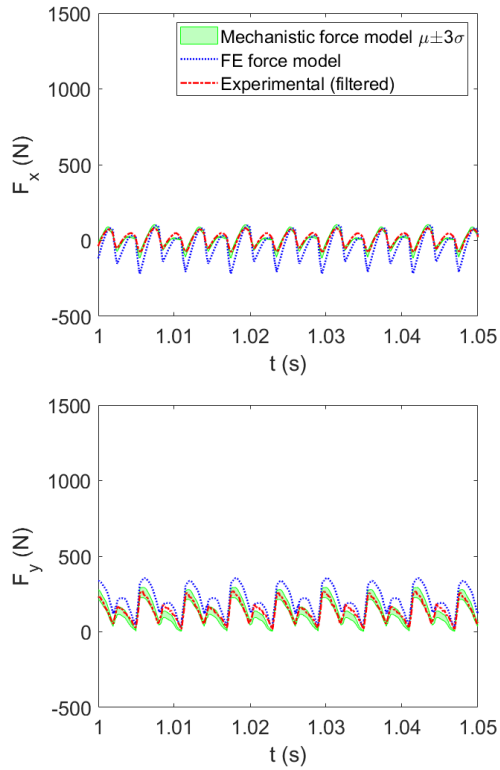


FIGURE 10. 6.35 mm radial depth (50% radial immersion), 0.075 mm/tooth, 2 mm axial depth.

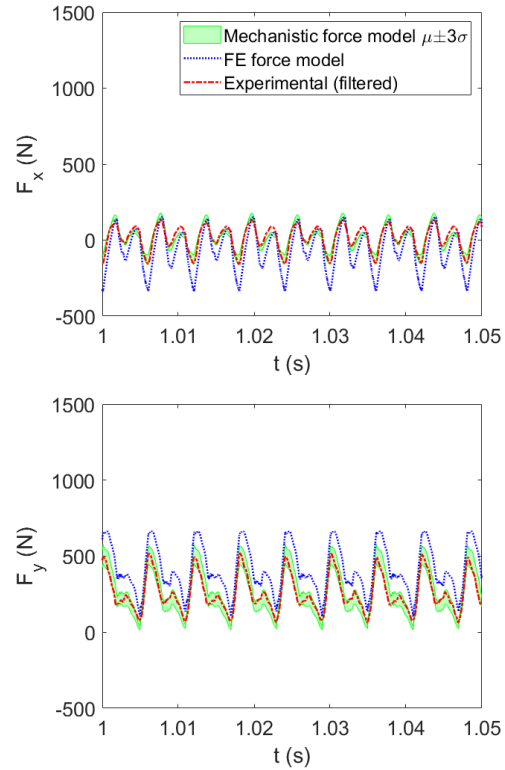


FIGURE 11. 6.35 mm radial depth (50% radial immersion), 0.075 mm/tooth, 4 mm axial depth.

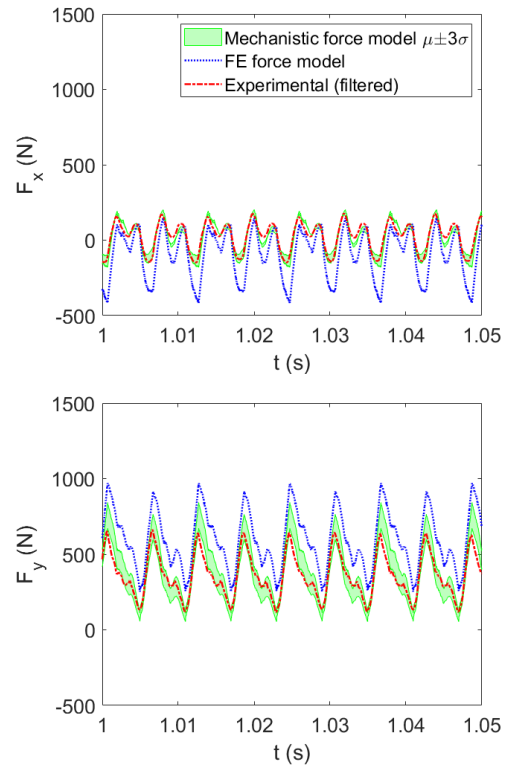


FIGURE 12. 6.35 mm radial depth (50% radial immersion), 0.075 mm/tooth, 6 mm axial depth.

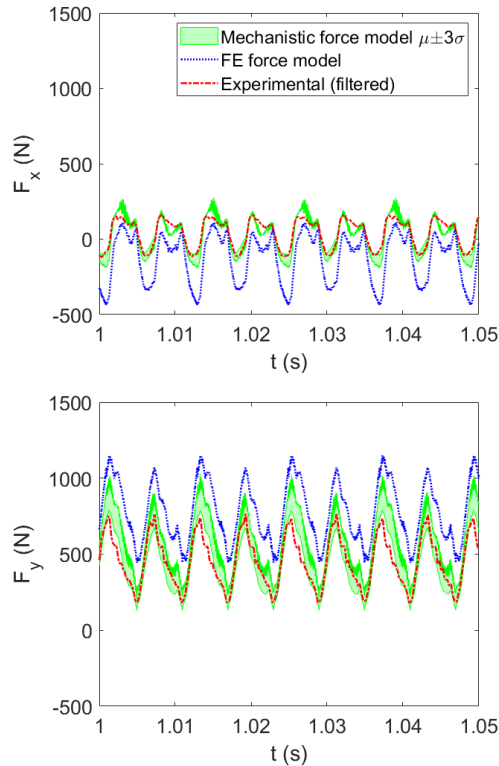


FIGURE 13. 6.35 mm radial depth (50% radial immersion), 0.075 mm/tooth, 8 mm axial depth.

For the results displayed in Figs. 10 through 13, it is seen that the measured force profiles are contained within the \pm three standard deviation error bounds from the linear regression identification of the cutting force coefficients. The finite element-based predictions overpredict the force levels in both the x and y directions

CONCLUSIONS

This paper describes a case study for using structured light scanning to predict cutting forces for a non-standard geometry endmill. The measured cutting edge geometry was incorporated into a time domain simulation used to predict the milling forces. Two methods were used to derive the force models: 1) experimental cutting tests; and 2) orthogonal finite-element cutting simulations. The predicted forces were validated with cutting tests performed at varying axial depths of cut. Good agreement between predicted and measured cutting forces for both force models (experimental and finite element-based) was obtained. This digital force modeling approach can be used for any endmill geometry and peripheral milling process.

REFERENCES

1. No, T., Gomez, M., Copenhaver, R., Uribe Perez, J., Tyler, C., and Schmitz, T., 2019, Force and Stability Modeling for Non-standard Edge Geometry Endmills, *Journal of Manufacturing Science and Engineering*, 141(12): 121002.
2. No, T., Gomez, M., Copenhaver, R., Uribe Perez, J., Tyler, C., and Schmitz, T., 2019, Scanning and Modeling for Non-standard Edge Geometry Endmills, *Procedia Manufacturing*, 34: 305–315.
3. No, T., Gomez, M., Copenhaver, R., and Schmitz, T., 2019, Structured light scanning for endmill modeling, *American Society for Precision Engineering Annual Meeting*, October 28–November 1, Pittsburgh, PA.
4. Gomez, M., No, T., Smith, S., and Schmitz, T., 2020, Cutting Force and Stability Prediction for Inserted Cutters, *Procedia Manufacturing*, 48: 443-451.
5. Gomez, M., No, T., and Schmitz, T., 2020, Digital Force Prediction for Milling, *Procedia Manufacturing*, 48: 873-881.
6. No, T., Gomez, M., Smith, S., and Schmitz, T., 2020, Cutting Force and Stability for Inserted Cutters using Structured Light Metrology, *Procedia CIRP*, 53rd CIRP Conference on Manufacturing Systems, July 1-3, 2020, Chicago, IL.
7. No, T., Gomez, M., Karandikar, J., Heigel, J., Copenhaver, R., and Schmitz, T., 2021, Contributions of Scanning Metrology Uncertainty to Milling Force Prediction, *Procedia Manufacturing*, 53: 213-222.
8. No, T., Gomez, M., and Schmitz, T., 2021, Propagation of Johnson-Cook Flow Stress Model Uncertainty to Milling Force Uncertainty using Finite Element Analysis and Time Domain Simulation, *Procedia Manufacturing*, 53: 223-235.
9. Titu, N.A., Baucum, M., No, T., Trotsky, M., Karandikar, J., Schmitz, T.L. and Khojandi, A., 2021, Estimating Johnson-Cook Material Parameters using Neural Networks, *Procedia Manufacturing*, 53: 680-689.
10. Schmitz, T. and Smith, K.S., *Machining Dynamics: Frequency Response to Improved Productivity*, Second Edition, Springer, New York, NY, 2019.